Malan, Willem Dutoit; Akdogan, Guven; Taskinen, Pekka; Hamuyuni, Joseph; Zietsman, Johan

Phase equilibria and thermodynamic evaluation of the Fe-V-O system in air

Published in:
Calphad: Computer Coupling of Phase Diagrams and Thermochemistry

DOI:
10.1016/j.calphad.2018.08.003

Published: 01/12/2018

Document Version
Peer-reviewed accepted author manuscript, also known as Final accepted manuscript or Post-print

Phase equilibria and thermodynamic evaluation of the Fe-V-O system in air

Willem Dutoit Malan[a], Guven Akdogan[b], Pekka Taskinen[c], Joseph Hamunyani[c], Johan Zietsman[a]

[a]*Department of Material Sciences and Metallurgical Engineering, University of Pretoria, Private Bag X20, Hatfield, 0028, South Africa*
[b]*Department of Process Engineering, Stellenbosch University, Banghoek Rd, 7599, South Africa*
[c]*Metallurgical Thermodynamics and Modelling, School of Chemical Engineering, Aalto Unviersity Vuorimiehentie 2K, FI-00076 Aalto*

Abstract

The Fe-V-O system in air was studied experimentally ranging from 700 °C to 1450 °C by high-temperature equilibration, quenching, scanning electron microscope and microprobe analysis. The thermodynamic evaluation was performed with FactSage 7.0. The solubility of V_2O_5(s) in Fe_2O_3(s) was described with the compound energy formalism. The properties of the liquid phase were described with both the quasichemical model and the associate species model. A set of self-consistent thermodynamic parameters were estimated within acceptable error limits. The calculated phase diagram of Fe-V-O in air is presented and compared to experimental observations and other literature data.

Key words: Fe-V-O system, thermodynamics, static experiments, phase diagram

1. Introduction

The Fe-V-O system has become notably important for understanding the corrosion mechanism of vanadium-based resistant steels, the processes used to treat vanadium-containing metallurgical slag, and fouling and ash build-up thermal power plants [1, 2]. Another reason for its importance is the low solidus temperature of V_2O_5-containing oxides, which can form liquids down to 650 °C and consequently destroy protective oxide layers [3].

Since Fe and V have 2 and 4 valence states, respectively, a substantial number of stable compounds and solid solutions exist over a wide range of oxygen partial pressures. For this reason, this investigation was limited to the stability range of Fe-V-O in air.

A number of studies have investigated phase equilibria between V_2O_5 and Fe_2O_3 in air and in pure oxygen up to 900 °C[4, 5, 1, 2]. In these experimental investigations phase equilibria were established with dynamic techniques, such as DTA (differential thermal analysis), TGA (thermogravimetric analysis) or DSC (differential Scanning calorimetry). However, these techniques are limited to systems with fast phase changes, and in any system with sluggish kinetics, it is possible that a system would not reach chemical equilibrium and this may result in spurious observations [6].

This study therefore focused on resolving phase equilibria contradictions from previous experimental studies from 700 °C to 1450 °C by means of the equilibration and rapid quenching technique. Liquidus and solidus composition were determined, eutectic and peritectic temperatures and compositions were estimated where possible and solid state equilibria of stoichiometric compounds were investigated. Furthermore, the system was thermodynamically assessed on the basis of the FToxid database utilizing well-known CALPHAD (calculation of phase diagrams) methods. All calculations were done with FactSage 7.0 [7]. The study is part of an effort to characterise and model multi-component systems containing V_2O_5.

2. Literature Data

2.1. Structure and Phase Transformation

Two vanadate compounds have been reported between Fe_2O_3 and V_2O_5, namely $FeVO_4$ (orthovanadate) and $Fe_2V_4O_{13}$. The 1:1 Fe:V mole ratio othovanadate belongs to the space group P1 and have been detected by numerous authors with X-ray diffraction [4, 5, 8, 9, 1, 2]. The compound presents four high-pressure phases labelled, I,II, III and

IV [10]. Phase I is less dense and stable under atmospheric conditions. The other three $FeVO_4$ phases are classified by increasing density. The transition of I - II, II - III and III - IV has been observed by Hotta et al. [11] at 800 °C and 5.5 GPa. This finding suggests that $FeVO_4$-I is stable under the thermodynamically favourable conditions used in this study, given that all experiments and assessments were conducted at 1 atm. Furthermore, it is known that the compound melts incongruently and that the melting behaviour of $FeVO_4$ depends greatly on the synthesis conditions, but primarily on the partial pressure of oxygen. That said, the amount of disorder in the crystal lattice affects the incongruent melting point. This phenomena was confirmed by Fotiev et al. [1], who noted that changing the oxygen partial pressure from 1 atm to 0.211 atm depressed the melting range by 20 K. Moreover, $FeVO_4$ is stable under oxidising conditions, and decomposes according to Equation 1 when the partial oxygen pressure is lowered [3]:

$$2\,FeVO_4(s) \longrightarrow Fe_2O_3(s) + 2\,VO_2(s) + 0.5\,O_2(g) \tag{1}$$

The second vanadate, $Fe_2V_4O_{13}$, has a single paramagnetic phase that belongs to the space group $P2_1/c$, and was detected by Pletnev et al. [12], Permer and Laligant [13] using NMR (nuclear magnetic resonance). Wang et al. [14] used a flux method from a starting mixture of 95% V_2O_5 and 5% Fe_2O_3 to prepare the compound, while Si et al. [15] used a liquid precipitation method to synthesize it. The starting materials, $Fe(NO_3)\cdot H_2O$ and NH_4VO_3 were dissolved in distilled water at molar ratios of Fe:V = 1:2 and stirred for 3 hours in a ultrasonic instrument. The precipitate was separated by centrifugation, followed by washing and drying for an extended period. A final calcining step was employed at 300 and 400 °C to obtain $Fe_2V_4O_{13}$. The compound was analytically identified with XRD (X-ray diffraction) and SEM-EDS (scanning electron microscope with energy dispersive spectrometry). It has a monoclinic structure, and melts incongruently [2, 1]. Furthermore, the liquidus temperature of the compound decreased by roughly 28 K when oxygen partial pressure was changed from 1 atm to 0.21 atm.

The structures of V_2O_5 and Fe_2O_3 are orthorhombic and tetragonal, respectively, and both compounds have been described well in numerous experimental investigations and thermodynamic assessments [16, 17, 18, 19, 20, 21, 22].

2.2. Liquidus and solidus data

The methods of investigation and invariant points from previous studies are presented in Table 1. The invariant points of Kerby and Wilson [5] are unusual and controversial, attributed to their observation that the compounds, Fe_2O_3(s) and $FeVO_4$(s) melted within a liquid miscibility gap. An inspection into instability of a single liquid phase revealed that for a liquid-liquid miscibility gap to appear, like interactions (i-i, j-j) need to be significantly stronger than unlike interactions (i-j) [23]. This is normally the case with silica systems, where an SiO_2 component is chemically very different compared to many other metal oxides. In these systems, attraction between like molecules (i-i, j-j) is stronger than the unlike molecules (i-j). Albeit that no experimental evidence exists to determine interaction strength in a Fe-V-O slag, it is unlikely that such melting behaviour would occur, because in principle, Fe and V ions based on their ionic radii are chemically similar [24]. On the basis of chemical similarity, it is assume that attraction between unlike molecules (Fe-V) are stronger than attraction between like molecules (Fe-Fe, V-V). Furthermore,no liquid-liquid miscibility gap was observed in the results of this study (See Results) or any of the other reported studies of Fe-V-O system in air [1, 2]. Therefore it was decided to exclude the liquidus and solidus data of Kerby and Wilson [5] from the thermodynamic assessment.

The reported invariant point data from the studies of Fotiev et al. [1], Walczak et al. [2] were given identical weight contribution in the assessment. Both studies identified and included the compound, $Fe_2V_4O_{13}$ and reported good agreement with the accepted melting point (669.85 °C) of V_2O_5 [7]. Some differences of invariant points were however noted. For example, a transition temperature of the invariant reaction, $FeVO_4 \rightarrow$ Liquid + Fe_2O_3, ranging from 840 °C to 870 °C has been postulated. Liquidus and solidus temperature lines have also not corresponded, with Walczak et al. [2] reporting a higher solubility of Fe_2O_3 in the slag at corresponding temperatures. Walczak et al. [2] even included a solubility range of Fe_2O_3 in V_2O_5, which was first suggested by Burzo. and Stanescu [25] and later detected by Burzo. and Stanescu [26], Palanna et al. [27]. The liquidus data above the $FeVO_4$ peritectic point have been extrapolated in all previous studies and was not considered in the assessment.

2.3. Thermodynamic data

The enthalpies of formation and standard entropies of $FeVO_4$(s) and $Fe_2V_4O_{13}$(s) were obtained from EMF measurements [28, 29, 30]. The heat capacities of both compounds were determined calorimetrically by Cheshnitski et al.

Table 1: Invariant reactions and phase transitions in the Fe−V−O system in air from literature.

Method	Composition (V_2O_5 mole %)	Temperature °C	Type of invariant	Equilibrium solid phases	Reference
DTA and X-Ray	89	634	Eutectic	V_2O_5, $FeVO_4$	[4]
Diffraction	37	843	Peritectic	Fe_2O_3, $FeVO_4$	[4]
DTA and X-Ray	80	645	Eutectic	V_2O_5, $FeVO_4$	[5]
Diffraction	64	843	Peritectic	$FeVO_4$	[5]
	40	843	Peritectic	$FeVO_4$	[5]
	38	645	Eutectic	Fe_2O_3, $FeVO_4$	[5]
DTA and X-Ray	97	658	Eutectic	V_2O_5, $Fe_2V_4O_{13}$	[1]
Diffraction	93	692	Peritectic	$FeVO_4$, $Fe_2V_4O_{13}$	[1]
	85	870	Peritectic	$FeVO_4$, Fe_2O_3	[1]
DTA and X-Ray	96	615	Eutectic	V_2O_5, $Fe_2V_4O_{13}$	[2]
Diffraction	91	665	Peritectic	$FeVO_4$, $Fe_2V_4O_{13}$	[2]
	80	850	Peritectic	$FeVO_4$, Fe_2O_3	[2]

[31] in temperatures ranging from 298 K to 973 K. Moreover, the heat capacity of $FeVO_4$ was similarly determined in a low temperature range from 60 K to 300 K by Borukhovich et al. [32], who used X-ray diffraction and spectroscopic analysis to study the single phase nature of the sample.

An inspection of Equation 10 revealed that thermodynamic data of Fe_2O_3(l) was required to describe the slag phase with both the modified quasichemical model and the associate species model. However, in reality, the Fe_2O_3(l) compound does not exist because of hematite's solid state transition to magnetite at 1388.73 °C in air (Equation 2). The transition temperature was determined with FactSage 7.0.

$$3\,Fe_2O_3(s) \longrightarrow 2\,Fe_3O_4(s) + 0.5\,O_2(g) \tag{2}$$

At oxidizing conditions, the slag in any Fe-M-O (M = Metal) system predominantly contains Fe^{3+} ions surrounded by O^{2-} molecules. Although it was mentioned that Fe_2O_3(l) does not exist, theoretically it needs be part of the calculation to model Fe^{3+} solubility in a V-O slag. The theoretical Fe_2O_3(l) thermodynamic data was not available in the FACTPS database and was taken from the study of Kowalski and Spencer [33], but was slightly adjusted in this study to reproduce experimental data within acceptable limits. Thermodynamic data of all other stable compounds of the Fe-V-O system in air were taken from the FactPS database [7]. The data of all stable compounds used in this study are summarized in Table 5. This data were used in the optimization, with minor adjustments made to $\Delta H^{\circ}_{f,298}$ and S°_{298} values of $FeVO_4$(s), $Fe_2V_4O_{13}$(s) and Fe_2O_3(l) to reproduce experimental data (see Thermodynamic Calculations).

3. Experiments

3.1. Sample Preparation

The starting materials used for the experiments were V_2O_5(s) and Fe_2O_3(s). The material, source and purity are presented in Table 2. Mixtures of selected bulk compositions of less than 0.4 g were prepared by weighing the oxide powders, followed by mixing them thoroughly using an agate mortar and pestle. Prepared samples had an initial composition to allow for a liquid and a solid phase to be in equilibrium at a desired temperature. The sample were pelletised at 20 MPa.

Table 2: Purity of initial materials and sources they were acquired from.

Material	Source	Purity
Divanadium Pentaoxide	SIGMA ALDRICH, RSA	99.60%
Ferric Oxide	SIGMA ALDRICH, RSA	>99 %

The $Fe_2V_4O_{13}$ phase was mostly undetected by previous studies of Fe-V-O in air, supposedly due to it's slow formation. Another contributing factor that has been postulated by Walczak et al. [2] is the undefined X-ray pattern of this phase, which had been difficult to distinguish from X-ray patterns of V_2O_5, Fe_2O_3 and $FeVO_4$. The latest studies of Fotiev et al. [1] and Walczak et al. [2] did however identify the X-ray pattern of the compound and was brought about by synthesizing a mixture of Fe_2O_3 and V_2O_5 with a molar ratio of 1:2 at temperatures ranging from 600 °C to 620 °C. This approach was also used in this study. The compound was calcined for 72 hours in a muffle furnace at 600 °C, then slowly cooled, ground, and pelletized again. After three such cycles the sample was mounted in epoxy and prepared for SEM-EDS analysis and EPMA (Electron Probe Micron-Analyser) using standard metallographic techniques. Furthermore, an attempt to understand the sluggish reaction mechanism of $Fe_2V_4O_{13}$ was made by varying synthesis time and starting composition of V_2O_5 and Fe_2O_3 from 80 mol % V_2O_5 down to 55 mol % V_2O_5.

3.2. Experimental Procedure

Equilibration experiments were conducted in a vertical electrical resistance tube furnace (Lenton, UK) with a 35 mm inner diameter alumina work tube. Before any equilibration experiments were conducted, a thermal profile of the tube furnace was determined at 700 °C, 1000 °C and 1300 °C. S-type thermocouples were used to measure temperature, and these thermocouples were calibrated according to the melting point of copper. This calibrated S-type thermocouple was connected to a Keithley 2010 DMM multimeter (Cleveland, OH, USA), and a cold junction compensation was connected to a Keithley 2000 multi-meter (Cleveland, OH, USA) to measure the ambient temperature with a PT100 sensor (Platinum Resistance thermometer, SKS Group, Finland). The temperature was measured and logged every two seconds with an NI labVIEW temperature logging program.

As an example, the furnace was set at 1000 °C and once temperatures close to 1000 °C were measured, a small hot zone of 4 cm to 5 cm in length was marked. The temperature in the hot zone did not deviate more than 2 °C. The zone is indicated on Figure 1a as two dashed lines within the working alumina tube.

All specimens were suspended in the furnace with Pt wire and wrapped in a Pt envelope. The hand-assembled envelope was chosen over Pt foil, given that small voids in the envelope will allow the sample to come in direct contact with the quenching medium. The relatively high surface tension of the slag and the shape of the Pt envelope did contain the aggressive slag. Pt serves as inert substance due to its low affinity for oxygen and it therefore did not react with the oxide specimen. Its high melting temperature (1770 °C) also made it possible to conduct experiments over the desired temperature range of this study.

The specimen was introduced into the furnace from the bottom by slowly pulling on the wire from the top of the furnace. The slag behaved extremely aggressively which can be due experimental temperatures being well above the melting temperature of V_2O_5 and causing a superheated V-O slag to form. A systematic increase in temperature was therefore required to contain the aggressive slag. The specimen was allowed to melt slowly by keeping the sample in a lower temperature area of the furnace for 30 to 45 s before finally raising it into the hot zone.

Equilibrium conditions were confirmed by comparing similar samples from different time intervals to each other, assessing the compositional homogeneity of the phases by EPMA, and approaching equilibrium from different temperature directions. The oxides, V_2O_5(s) and Fe_3O_4 melt at 669.85 °C and 1596.85 °C respectively. This large difference made it necessary to do experiments over a wide temperature range. For this reason, the equilibration time was determined at 800 and 1200 °C. At 800 °C, time intervals were chosen as 4, 8, 16, 24 and 48 hours. Once the equilibration time was established, a series of time intervals were determined at 1200 °C. Equilibration is dependent on temperature due to transport and reaction kinetics being faster at higher temperatures. Other factors, such as solid-liquid surface tension, liquid viscosity and density have a lesser effect on equilibration time. Confirmation of equilibrium was done prior to experiments at other temperatures.

Samples were quenched releasing the specimen rapidly into a beaker of ice water or brine, situated no more than 10 mm from the exterior of the alumina working tube. The specimen was rapidly removed from the beaker and dried with compressed air to minimize the probability of dissolving the sample in water.

The specimen was then mounted in epoxy resin. The mounted sample was ground and polished to expose a suitable cross section. Dry grinding was used to prevent V_2O_5 from dissolving, since it has a solubility of 0.8 g L^{-1} in water [34].

The polished samples were carbon coated with a Leica EM SCD050 Coater (supplied by Leica Mikrosysteme GmbH, Vienna), before EPMA (Cameca SX 100). Carbon coating avoids charge build-up of a specimen, which

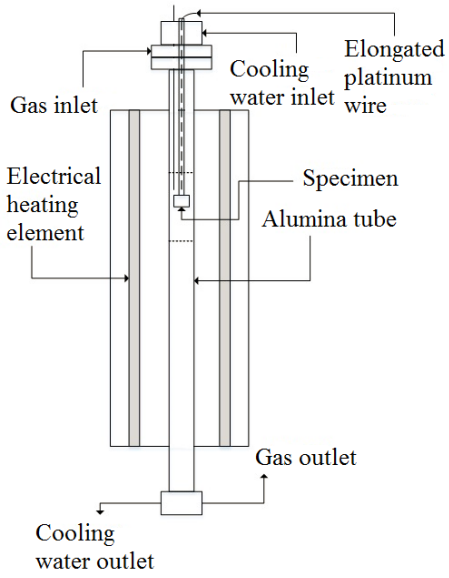

(a) Schematic of the vertical front view section of the furnace and auxiliaries.

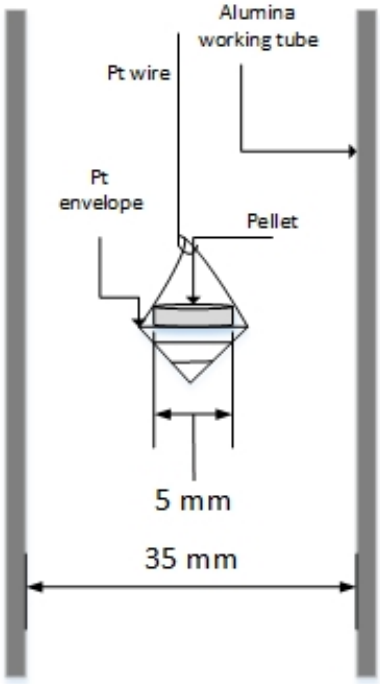

(b) Envelope design and suspension of the pellet in the furnace.

Figure 1: Furnace and suspension design.

reduces thermal damaging of samples and improves secondary electron signals, thereby improving imaging. The samples were analysed at 15 kV accelerating voltage and 40 nA beam current. All elements were measured on their Kα lines, using wavelength-dispersive spectrometers. Fe was calibrated on Fe_2O_3, V on pure V, but the measured V mass fractions were adjusted as if V had been calibrated on vanadinite ($Pb_5(VO_4)_3Cl$). This was done to better match the matrix of the calibration standard with the (oxidic) matrix of the samples. The matrix correction in the probe software was based on the "X-PHI" model [35].

3.3. Application of the Phase Rule

In any system at equilibrium, homogeneous or heterogeneous, the number of fixed experimental variables are limited by the Gibbs phase rule (Equation 3). The phase rule allows for the unambiguous determination of the thermodynamic state of a system by fixing a number of intensive variables after identifying the number of components and phases.

$$\mathrm{f} = \mathrm{c} - \mathrm{p} + 2 \tag{3}$$

where c is the number of components and p is the number of phases. For the system under investigation, the pressure is fixed at 1 atm (isobaric conditions). The phase rule equation therefore reduces to Equation 4.

$$\mathrm{f} = \mathrm{c} - \mathrm{p} + 1 \tag{4}$$

In this case, $c = 4$ (V, Fe, O and N), and $p = 3$ (solid oxide, liquid slag, and gas). Although the gas phase contains small quantities of other gaseous species, such as, CO, CO_2, H_2O and Ar, their partial pressures are very low compared to O_2 and N_2. These can therefore be assumed to have negligible effect on the behaviour of our system. According to Equation 4, for these conditions $f = 2$. Experiments for the Fe-V-O in air were undertaken with the bottom and top of the working tube left open to the atmosphere. The air composition fixed the partial pressure of O_2, an intensive property, at 0.21 atm, which reduced f by one. Temperature, another intensive variable, was fixed at the furnace set-point during experiments, which reduced f by one again. This left the system fully defined, and invariant (f = 0). As a result, the equilibrium liquid and solid compositions could be determined unambiguously knowing that the system state had been defined completely.

4. Thermodynamic modelling

4.1. Stoichiometric Compounds

The standard Gibbs energies of stoichiometric compounds and solution phase constituents are expressed in the form of $\mathrm{G} - \sum \mathrm{H_{SER}}$ and also as a function of temperature. The $\sum H_{SER}$ (Standard Element Reference) is the sum of enthalpies of the elements at 298 K and 1 bar pressure and was also the reference state for calculations in this study. The data of pure compounds are obtained from critical analysis and computer optimization of experimental spectroscopic heat capacity, enthalpy, entropy, and Gibbs energy data, as well as from studies of phase equilibria [36]. For thermodynamic assessment purposes, the standard Gibbs energy of stoichiometric compounds are described by:

$$\mathrm{G^{\circ}(T)} = \left(\Delta \mathrm{H_{f,298K}} + \int_{298\mathrm{K}}^{\mathrm{T}} \mathrm{C_p(T)dT}\right) - \mathrm{T}\left(\mathrm{S^{\circ}_{298K}} + \int_{298\mathrm{K}}^{\mathrm{T}} (\mathrm{C_p(T)/T)dT}\right) \tag{5}$$

The parameters in Equation 5 are optimized from selected literature data reviewed in Literature Data. For enthalpy of formation, standard entropy and heat capacity equation coefficients of $FeVO_4$(s) and $Fe_2V_4O_{13}$(s) obtained from experimental studies by Volkov [29], Cheshnitski et al. [31] had to be adjusted slightly to accurately reproduce reported invariant reactions of the Fe-V-O system in air.

4.2. Gas Phase

The system pressure was kept constant at approximately 1 atm (absolute) for all experiments and modelling efforts. The gas phase was therefore assumed to exhibit ideal behaviour. This assumption is justified by the limiting condition in Equation 6 [37]:

$$\lim_{\mathrm{P}\to 0} \frac{f_i}{p_i} \equiv 1 \tag{6}$$

Equation 6 states that as pressure approaches zero, all gasses behave ideally. The molar Gibbs energy of the gas phase is given by Equation 7 [37]. P_0 is the standard pressure of 1 atm and P_i is the partial pressure of gaseous specie *i*.

$$G_m = \sum_i X_i G_i^\circ + RT \sum_i X_i ln X_i + RT ln(P_i/P_\circ) \tag{7}$$

4.3. Liquid Phase

4.3.1. Quasichemical Model

The modified quasichemical model (MQM) [38, 39], which takes into account short range ordering of second nearest neighbours have recently been used by Xie et al. [40] to describe the liquid phase in a PbO-V_2O_5 system. It was assumed that liquid V_2O_5 is made up of the building unit VO_4^{3-}, which in turn corresponded to VO^{3+} cation specie. It was however stated by Xie et al. [40], that $V_2O_7^{4-}$ can also be used as a building unit. Describing the V_2O_5 melt with these building units, was accepted from the study of Kawakita et al. [41], which investigated the local structures of liquid and vitreous V_2O_5 and P_2O_5 melts. A similar finding was made by Hawakawa and Yoko [42], who in turn investigated the structure of lead vanadate glasses. Moreover, it was found from the study of Kawakita et al. [41] that the characteristics of liquid P_2O_5 is similar to liquid V_2O_5. Hudon and Jung [43] and Rahman et al. [44] then successfully adopted $P_2O_7^{4-}$ as building unit of P_2O_5 in the $CaO-P_2O_5$ and $SiO_2-P_2O_5$ systems, respectively. This approach has also been adopted by FactSage for describing slag phases containing P_2O_5 [7].

To remain consistent with modelling methods of the FToxide database in FactSage, liquid V_2O_5 will have the building unit $V_2O_7^{4-}$, which postulates V can be surrounded by four broken oxygen atoms. As a result, $V_2O_3^{4+}$ is used as the corresponding cation specie. Each cation specie has a corresponding coordination number, Z. According to the existing FactSage FTOxid database, the divalent Z is always set at 1.3774 and all other cation coordination numbers are calculated according to the ratio, $\frac{1.3774}{2} = \frac{Z_{A^{A+}}}{charge}$. Where $A+$ represents the charge of a cation specie. The quasichemical reaction between cations in liquid Fe-V-O in air can be expressed as:

$$(Fe-Fe) + (V_2O_3 - V_2O_3) = 2(Fe - V_2O_3) \qquad \Delta g_{Fe-V_2O_3} \tag{8}$$

where $\Delta g_{Fe-V_2O_3}$ is the molar Gibbs energy of reaction 8 where, Fe can be in the form of Fe^{2+} or Fe^{3+}. However, Fe^{2+} concentration is generally low at oxidative conditions and will have only a small influence on the liquidus composition at higher overall Fe concentration and for this reason, the binary pair fraction $FeO-V_2O_5$ was considered to behave ideally. Overall, there will be 3 second nearest neighbour pair reactions. Optimized parameters for the binary FeO-Fe_2O_3 slag solution were taken from Degterov et al. [21]. The molar Gibbs energy of the respective $FeO-V_2O_5$ and $Fe_2O_3-V_2O_5$ solutions are expressed as follows:

$$G_m = n_{FeO} g^\circ_{FeO} + n_{V_2O_5} g^\circ_{V_2O_5} - T\Delta S^{config} + n_{Fe-V_2O_3}(\Delta g_{Fe-V_2O_3}/2) \tag{9}$$

$$G_m = n_{Fe_2O_3} g^\circ_{Fe_2O_3} + n_{V_2O_5} g^\circ_{V_2O_5} - T\Delta S^{config} + n_{Fe-V_2O_3}(\Delta g_{Fe-V_2O_3}/2) \tag{10}$$

where,ΔS^{config} is the configuration entropy expressed as random mixing of the bonds over bond sites in one dimension (Ising approximation) [45]. Moreover, $\Delta g_{Fe-V_2O_3}$, can be expanded as an empirical polynomial function in the mole fractions of pairs.

$$\Delta g_{Fe-V_2O_3} = \Delta g^\circ_{Fe-V_2O_3} + \sum_{i\geq 1} g^{i0}_{Fe-V_2O_3} X^i_{Fe-Fe} + \sum_{j\geq 1} g^{0j}_{Fe-V_2O_3} X^j_{V_2O_3-V_2O_3} \tag{11}$$

where Fe represents Fe^{2+} and Fe^{3+} cations. $\Delta g^0_{Fe-V_2O_3}$, $g^{i0}_{Fe-V_2O_3}$ and $g^{0j}_{Fe-V_2O_3}$ are temperature dependent adjustable model parameters optimized to reproduce the liquidus within acceptable error limits.

The $\Delta g^\circ_{Fe-V_2O_3}$ term has a major influence at composition of maximum short range ordering. It is known that maximum short range ordering usually occurs at the intermediate compound with the highest melting point (congruent melting) and the minimum mixing enthalpy. This was the findings from the recent studies of Xie et al. [40], Hudon and Jung [43], N.Wang [46], Protstakova et al. [47]. However, it is known that no intermediate compounds in the Fe-V-O system in air melts congruently, hence the $\Delta g^\circ_{Fe-V_2O_3}$ term may have a less significant impact on the Gibbs

energy of the liquid phase. It is therefore expected that non-ideal behaviour of the liquid phase can be sufficiently described by the terms, $g^{i0}_{Fe-V_2O_3}$ and $g^{0j}_{Fe-V_2O_3}$. Moreover, it is known when the total mole fraction of V_2O_5 is $<< 1/2$, $X_{V_2O_3-V_2O_3}$ will be small and $g^{0j}_{Fe-V_2O_3}X_{V_2O_3-V_2O_3}$ will have a small effect on the Gibbs energy of the liquid. In this region, only the parameters $g^{i0}_{Fe^{3+}-V_2O_3}$ will largely contribute to the Gibbs energy. The opposite is true when the total mole fraction of V_2O_5 is $>> 1/2$ [45].

Furthermore, a ternary pair, $Fe_2O_3-FeO-V_2O_5$ exist from describing the liquid phase with the quasichemical model. A Kohler-like interpolation method, which is symmetric in nature, will be used as an initial approach for estimating thermodynamic properties and phase diagram data from binary model parameters. This interpolation method is based on the assumption that all components are chemically similar and had previously successfully described slag phases of higher order systems [48, 7, 49, 50, 51].

4.3.2. Associate Species Model

It should be noted that other thermodynamic models can be used to describe the liquid phase. The associate species model (ASM) uses intermediate/associate species to account for non-ideal behaviour of a liquid phase species. The model was originally developed by Hastie, Bonnell and co-workers [52, 53, 54, 55]. This simple model has been used extensively with great success to describe the liquid phase and is easily expanded to multi-component systems. For our system neither $FeVO_4$(s) nor $Fe_2V_4O_{13}$(s) melts congruently and consequently, will not be used as associates. The model effectively reduces to a substitutional model, hence components of the liquid are V_2O_5, FeO and Fe_2O_3.

$$\begin{aligned} G_m =& X_{V_2O_5}G^{\circ}_{V_2O_5} + X_{Fe_2O_3}G^{\circ}_{Fe_2O_3} + X_{FeO}G^{\circ}_{FeO} \\ &+ RT(X_{V_2O_5}LnX_{V_2O_5} + X_{Fe_2O_3}LnX_{Fe_2O_3} + X_{FeO}LnX_{FeO}) + G^e_m \end{aligned} \tag{12}$$

Parameters representing interactions between Fe_2O_3, FeO and V_2O_5 are introduced by adopting a Redlich-Kister polynomial to model the liquidus curve close to V_2O_5(s), $Fe_2V_4O_{13}$(s) and $FeVO_4$(s). Therefore, the excess Gibbs energy is described by the following expression:

$$\begin{aligned} G^e_m = X_{V_2O_5}X_{Fe_2O_3}{}^0L_{V_2O_5-Fe_2O_3} + X_{V_2O_5}X_{FeO}{}^0L_{V_2O_5-FeO} + X_{FeO}X_{Fe_2O_3}{}^0L_{FeO-Fe_2O_3} + \\ X_{V_2O_5}X_{Fe_2O_3}{}^1L_{V_2O_5-Fe_2O_3}(X_{V_2O_5} - X_{Fe_2O_3}) \end{aligned} \tag{13}$$

The parameter L is a linear function of temperature, equated as ${}^iL = a + bT$ and $i = 1, 2, 3..n$. Kowalski and Spencer [33] successfully described the liquid phase of an Fe-O system with Fe, FeO and Fe_2O_3 as associates. A Redlich-Kister function was introduced to account for non-ideal behaviour between components. Therefore, the interaction term, ${}^0L_{FeO-Fe_2O_3}$ from their study was used in the optimization to model the liquidus curve in the Fe-O rich region.

4.4. Modelling Solid Solutions

Solid solutions in the studied system were developed within the framework of the compound energy formalism (CEF). [56, 57]. This means that a mathematical expression like the CEF is more general than the actual physical model and can be applied to various constituents with different behaviour in a phase. When such generalized expressions are obtained, it is referred to as a formalism . It has been proven that the CEF is well suited to model solid solutions with two or more distinct sub-lattices. Furthermore, it allows for cations and anions of different valance to mix in different sub-lattices, corresponding to the structure of a solid solution [23].

$$\mathrm{G_m} = \sum_{\mathrm{i}}\sum_{\mathrm{j}} \mathrm{X_i X_j G_{ij}} - \mathrm{TS_{config}} + \mathrm{G_e} \tag{14}$$

$\mathrm{X_i}$ and $\mathrm{X_j}$ represent the site fractions of constituents i and j on the first and second sublattices, respectively. $\mathrm{S_{config}}$ is the configurational entropy and is expressed as follow:

$$\mathrm{S_c} = -\mathrm{R}(\mathrm{n}\sum_{\mathrm{i}} \mathrm{X_i LnX_i} + \mathrm{n}\sum_{\mathrm{j}} \mathrm{X_j LnX_j}) \tag{15}$$

with n being the stoichiometric constant of each lattice and R the ideal gas constant.

4.4.1. Hematite Solid Solution

A dilute solid solution of V_2O_5 in Fe_2O_3 crystal structures exist (Hematite solid solution). The Gibbs free energy of this hematite solid solution (SS) was developed within the framework of the CEF (Equation 14). In the model, it was assumed that all cations mix in one lattice and all anions in a second lattice. Some vacancies are introduced into the cation sub-lattice for charge neutrality. Hematite-SS is represented by a mixture of V^{5+}, Fe^{3+}+ ions and vacancies on cation sites and oxygen being the only anion, in the second sub-lattice. It has the chemical formula $(V^{5+}, Fe^{3+}, Va)_2(O)_3$ with charged end-member species optimized to model V_2O_5 solubility in hematite. Therefore the excess term in Equation 14 was set to zero. A triangle plane with a neutral line is presented in Figure 2.

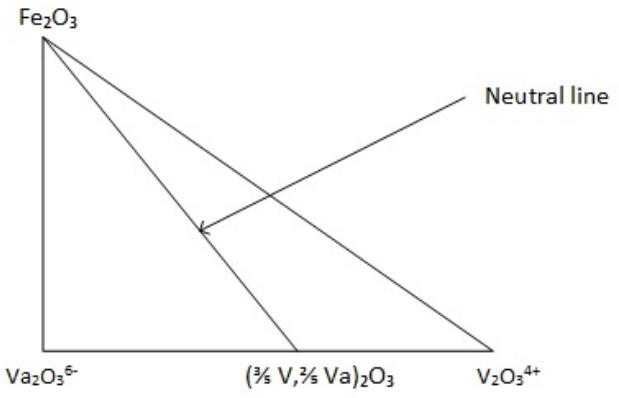

Figure 2: Schematic representation of end-member components and possible composition ranges on a neutral line of a Hematite solid solution

The apexes of the triangle in Figure 2 each represent an end-member and they have the following chemical formulas: $Fe_2^{3+}O_3^{2-}, V_2^{5+}O_3^{2-}[4+]$ and $Va_2O_3^{2-}[6-]$. The molar Gibbs energy of a hematite solid solution is expressed as follow:

$$\begin{aligned} G_{hem} = X_{Fe^{3+}}X_{O^{2-}}G^{\circ}_{Fe^{3+}:O^{2-}} + X_{V^{5+}}X_{O^{2-}}G^{\circ}_{V^{5+}:O^{2-}} + X_{Va}X_{O^{2-}}G^{\circ}_{Va:O^{2-}} + \\ +2RT(X_{Fe^{3+}}lnX_{Fe^{3+}} + X_{V^{5+}}lnX_{V^{5+}} + X_{Va}lnX_{Va}) + 3RT(X_{O^{2-}}lnX_{O^{2-}}) + G_e \end{aligned} \tag{16}$$

However, in Equation 16 two end-member components, $V_2^{5+}O_3^{2-}[4+]$ and $Va_2O_3^{2-}[6-]$, are electrically charged and cannot physically exist, but corresponding mathematical expressions can be derived from a combination of neutral components on Figure 2. The compound, $(\frac{3}{5}V, \frac{2}{5}Va)_2O_3$ on the neutral line in Figure 2 corresponds to 3/5 mole of V_2O_5(s), which in turn has a hematite-related structure. The neutral specie, $(\frac{3}{5}V, \frac{2}{5}Va)_2O_3$, which is a combination of the two electrically charged end-member components are expressed as follow:

$$3/5G^{\circ}_{V_2O_5(s)-Hem} = \frac{3}{5}G^{\circ}_{V^{5+}:O^{2-}} + \frac{2}{5}G^{\circ}_{Va:O^{2-}} + 2RT\left(\frac{3}{5}ln\frac{3}{5} + \frac{2}{5}ln\frac{2}{5}\right) \tag{17}$$

with, $G^{\circ}_{V_2O_5(s)-Hem} = G^{\circ}_{V_2O_5(s)} + A + BT$.

The third term in Equation 17 is an entropy of mixing contribution on the cation sub-lattice and A and B are optimised parameters. In addition, the end-members are derived, rearranged and expressed as follow:

$$G^0_{Va:O^{2-}Hem} = 0 \tag{18}$$

$$G^0_{V^{5+}:O^{2-}Hem} = G^0_{Hem-V_2O_5} - \frac{2}{3}G^0_{Va:O^{2-}} - \frac{10}{3}RT\left(\frac{3}{5}ln\frac{3}{5} + \frac{2}{5}ln\frac{2}{5}\right) \tag{19}$$

$$G^0_{Fe^{3+}:O^{2-}} = G^0_{Fe2O3(s)} \tag{20}$$

The terms, $G^0_{Va:O^{2-}Hem}$ are a reference term for other systems and have been set to zero [58]. The other term, $G^0_{V^{5+}:O^{2-}Hem}$ is optimized with respect to the standard enthalpy and entropy of formation of compound, V_2O_5(s) .

5. Sequence of Optimization

The principle of data fitting, assessment methodology and parameter optimization is based on a least-squares method. That is, an objective function is expressed as the difference between the calculated value of a given property and a experimental value of the same property. This difference is known as the residual. It is possible to acquire a set of optimized model parameters by minimizing the sum of the square of residuals over all measured points. The optimization was performed using the OPTISAGE tool in FactSage 7.0 which has the ability to consider all types of data simultaneously. The assessment methodology guidelines of Lukas et al. [23] were closely followed.

In the first step of optimization, the quasichemical temperature dependent parameters in Equation 11 were optimized to obtain a reasonable fit of the liquidus curve. The initial values of these parameters were set to zero, assuming ideal behaviour of the binary pairs, $FeO-V_2O_3$ and $Fe_2O_3-V_2O_3$. Moreover, at this step of optimization, the solid solution, Hematite, was modelled as pure Fe_2O_3(s). Thereafter, thermodynamic properties of the two vanadates, $Fe_2V_4O_{13}$(s) and $FeVO_4$(s) were slightly adjusted to reproduce peritectic transition temperatures.

Prior to the final step of optimization, the enthalpy of formation and standard entropy of $G^0_{V_2O_5(s)-Hem}$ from solid solution, Hematite, were optimized. In the final step of optimization all thermodynamic parameters were simultaneously optimized by considering all liquidus and solidus data. An identical approach was followed when using the associate species model to describe the liquid phase.

6. Results

6.1. Phase characterization and quantification

The polished and coated samples were analysed with EPMA and SEM-EDS, respectively. However, EPMA has been widely accepted as an analytical tool for high accuracy and precision quantification of liquid oxide phases [59]. Therefore EPMA is also preferred in this study due to its ability to quantify oxygen concentration in phases more accurately. However, EPMA and SEM-EDS provides only the total element content. The oxidation states of Fe and V were not analysed directly.

It was noted that O and V had overlapping X-ray emission peaks. Hence accuracy of quantitative analysis of oxygen concentration in the slag phase may be compromised. For this reason, oxygen concentration was calculated on the basis of stoichiometry (St.) by assuming V is in the 5+ and Fe in the 3+ oxidation state. At least ten points of each phase was analysed to calculate the standard deviation (σ) for each element. Furthermore, each experiment was repeated at least once to assert confidence in experimental set-up and procedure.

6.1.1. Synthesis of $Fe_2V_4O_{13}$

Some discrepancies in literature have been found regarding the existence and stability of the vanadate, $Fe_2V_4O_{13}$. It was therefore undertaken to thermally synthesize the compound at 600 °C to resolve some of the contradictions from previous studies. The synthesis were carried out in a muffle furnace and temperature in the furnace did not deviate more than 5 °C. Another advantage of having the synthesized vanadate compound is that it made it easier to determine the incongruent melting point in the Fe-V-O system in air due to the narrow temperature stability range of the compound when in equilibrium with the slag.

The method proposed and used by Walczak et al. [2] was followed, i.e. 3 cycles of 72 hours with repeated re-grounding, followed by SEM-EDS analysis. Different starting compositions are selected to try and gain a better understanding of the reaction mechanism and kinetics of the vanadate, $Fe_2V_4O_{13}$(s). The synthesis time and starting compositions of V_2O_5(s) to Fe_2O_3(s) are listed in Table 3.

Figure 3 presents polished sections of the synthesized samples at 24, 48, 96 and 216 hours. Two or three crystalline phases are always present and are identified with SEM-EDS as either V_2O_5(s) and $Fe_2V_4O_{13}$(s) or $FeVO_4$(s) and $Fe_2V_4O_{13}$(s), respectively. It is observed that 3 phases are present after, 24, 48 and 96 hours, and according to Equation 4, only 2 phases are allowed for a fully defined system. This implies that the system has not yet reached equilibrium and one phase had to be metastable.

The $FeVO_4$(s) phase appears to be less at 96 hours, when compared to an similar micro-image at 24 hours. After 216 hours of equilibration time, only small traces of the $FeVO_4$(s) phase was observed, suggesting that equilibrium was not reached due to mass transfer and other rate phenomena effects. This finding is further supported by a sample

Table 3: Experiments for the synthesis of $Fe_2V_4O_{13}$

Experiment	Temperature °C	V_2O_5 mole%	Fe_2O_3 mole %	Equilibration time (hr)
1	600	0.750	0.250	24
2	600	0.550	0.450	24
3	600	0.750	0.250	48
4	600	0.550	0.450	48
5	600	0.750	0.250	96
6	600	0.550	0.450	96
7	600	0.750	0.250	216
8	600	0.550	0.450	216
9	600	0.750	0.250	504
10	600	0.550	0.450	504

synthesized for 21 days, which revealed no traces of, $FeVO_4$(s). It is therefore likely that slow kinetics was the reason why some authors didn't detect, $Fe_2V_4O_{13}$(s) after very short equilibration times. This is especially relevant when dynamic experimental techniques that rely on fast phase transformations, were used to estimate liquidus and solidus temperatures.

In our investigation, $FeVO_4$(s) did form in the early stages of equilibration. This means that the first part of the mechanism ($V_2O_5 + Fe_2O_3 \rightarrow 2FeVO_4$) is fairly fast. However, the bulk composition and temperature placed the system in the $V_2O_5-Fe_2V_4O_{13}$ two-phase region. $Fe_2V_4O_{13}$ was then formed in the second step of the mechanism ($2FeVO_4 + V_2O_5 \rightarrow Fe_2V_4O_{13}$) and this step was significantly slower than first step of the mechanism. An identical mechanism was followed for a sample with an initial bulk composition of 55 mole % V_2O_5. However, in this case the bulk composition and temperature placed the system in the $FeVO_4-Fe_2V_4O_{13}$ two-phase region. Therefore, after 21 days, the products were $FeVO_4$(s) and $Fe_2V_4O_{13}$(s) and very little V_2O_5(s) was still present.

Furthermore, another important conclusion can be drawn. The solubility of Fe_2O_3(s) in V_2O_5(s) was lower then 1 %. This discovery contradicts the analytical observations of Walczak et al. [2], who suggested a solubility of 3 % at the eutectic temperature and between 2 and 3 % at 600 °C. However, all synthesized samples were air quenched and this can subsequently allow for Fe diffusion from the V_2O_5(s) lattice to form $Fe_2V_4O_{13}$(s). Nevertheless, this result is enough to substantiate our decision to neglect the small solubility range of Fe_2O_3(s) in the V_2O_5(s) crystal lattice during the assessment. This decision is further supported by Fotiev et al. [1] who ruled out a solubility of 3 % due to the presence of an eutectic composition of 2.5 % between V_2O_5(s) and $Fe_2V_4O_{13}$(s).

6.1.2. Liquidus and solidus

All analysed samples had two phases, a solid and liquid oxide. No immiscibility field in the liquid phase was observed in all analysed samples. Micrographs of phase assemblages are shown in Figure 4. Some scratches are seen on the images because of a dry polishing method used to avoid V_2O_5 dissolution in water. The raw EPMA data are found in Table 4. The standard deviation of each element is presented. It was noted that the raw data from SEM-EDS (not shown here) compared well to the raw data of EPMA. Complete homogeneity of molten phase was achieved in the equilibration and quenching. The raw data from EPMA were converted from V to V_2O_5 and Fe to Fe_2O_3 and then normalized. The normalized results were used in the thermodynamic assessment.

For the sample quenched at 800 °C, equilibrium was achieved after 16 hours. A slag phase and $FeVO_4$(s) were observed. Experimental results confirmed that $FeVO_4$(s) undergoes a peritectic transition between 850 and 860 °C to form hematite solid solution and molten slag. For the sample quenched at 1000 °C, the hematite solid solution and liquid slag phase were detected. All samples below 800 °C had an equilibration time of 48 hours and sample homogeneity was used to confirm equilibrium. The starting composition for the sample quenched at 700 °C was a mixture of the synthesized compound from Synthesis of $Fe_2V_4O_{13}$ plus a small percentage of V_2O_5(s). However, no traces of the orthovanadate, $Fe_2V_4O_{13}$(s) was detected after equilibration, indicating that the peritectic transition of $Fe_2V_4O_{13}$(s) to form molten slag phase and $FeVO_4$(s), is below 700 °C.

For the sample quenched at 1200 °C, equilibrium was achieved after 4 hours. An appreciable amount of precipi-

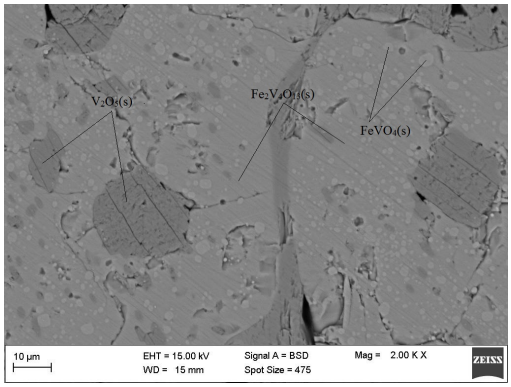

(a) 24 hours

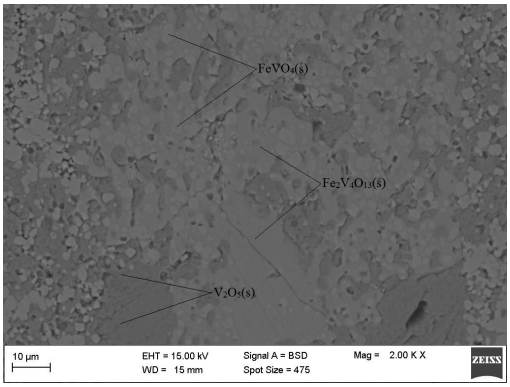

(b) 48 hours

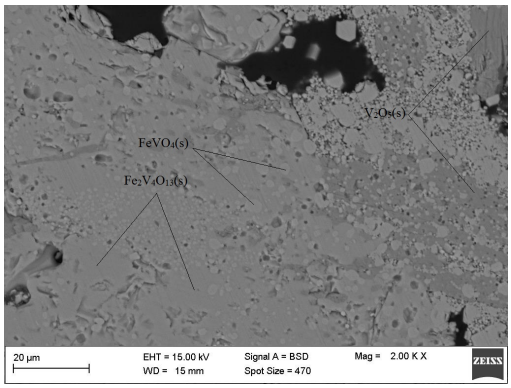

(c) 96 hours

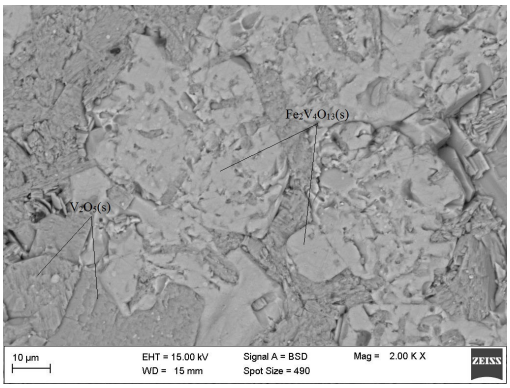

(d) 216 hours

Figure 3: BSE (Backscattered electrons) micrographs of $Fe_2V_4O_{13}$ synthesis samples prepared at 600 °C and an initial concentration of 75 mole % V_2O_5(s). Light crystals in (a), (b) and (c) are $FeVO_4$(s) and darker crystal phases wrapped around $FeVO_4$(s) are $Fe_2V_4O_{13}$(s). The darkest phase is V_2O_5(s)

.

Table 4: Summary of raw data of the quenched samples analysed with EPMA.

	Molten Phase						FeVO4(s)						Hematite-SS					
Temperature °C	Fe	Fe (σ)	V	V (σ)	O (St.)	Total	Fe	Fe (σ)	V	V (σ)	O (St.)	Total	Fe	Fe (σ)	V	V (σ)	O (St.)	Total
700	3.64	0.09	54.13	0.22	44.07	101.84	31.22	0.40	31.78	0.46	34.54	98.41						
750	5.88	0.28	52.73	1.19	43.94	102.55	31.86	0.31	32.38	0.42	35.56	100.54						
800 (SS)							31.84	0.30	31.99	0.67	34.55	99.35	68.72	0.49	1.05	0.67	30.36	101.29
800	8.44	0.49	50.51	0.31	43.29	102.24	31.52	0.14	31.99	0.11	35.15	98.90						
850	11.09	0.12	48.00	0.08	42.46	101.56	31.71	0.26	31.93	0.07	35.18	99.14						
860	12.49	0.16	47.06	0.22	42.32	101.87							68.36	0.19	2.06	0.13	31.00	101.42
900	13.67	0.61	46.61	0.39	42.48	102.76							68.91	0.21	1.50	0.22	30.79	101.20
950	15.66	0.17	44.65	0.12	41.79	102.10							67.29	0.64	1.54	0.07	30.13	98.96
1000	16.81	0.78	43.50	0.59	41.38	101.68							67.04	0.17	1.68	0.03	30.13	98.84
1050	17.87	1.50	42.33	1.05	40.92	101.11							66.90	0.28	2.07	0.21	30.37	99.34
1100	20.32	1.59	40.94	1.03	40.88	102.13							66.14	0.20	2.38	0.10	30.29	98.80
1150	21.53	1.68	40.05	1.02	40.70	102.28							66.42	0.09	2.64	0.17	30.62	99.68
1200	22.98	1.60	38.93	1.31	40.45	102.36							65.46	0.30	2.96	0.05	30.46	98.88
1250	26.42	2.02	36.12	1.90	39.72	102.26							66.17	0.28	3.77	0.14	31.40	101.34
1300	28.10	2.14	34.39	1.57	39.08	101.57							65.90	0.25	3.97	0.13	31.44	101.31
1350	31.20	2.09	33.19	1.14	38.82	103.21							63.32	0.36	4.35	0.19	30.63	98.30
1400	36.13	5.85	27.47	4.92	37.10	100.70							64.86	0.56	3.47	0.35	30.60	98.93
1450	N/A	N/A	N/A	N/A	N/A	N/A							67.16	0.42	2.50	0.07	30.82	100.48

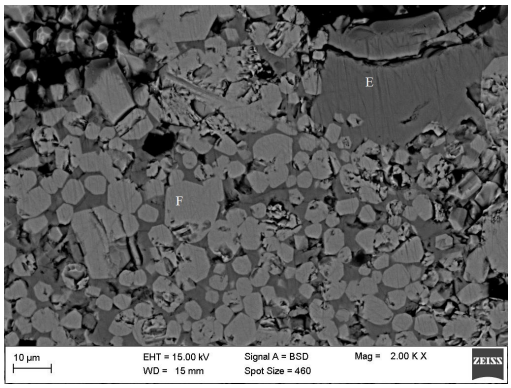

(a) 800 °C

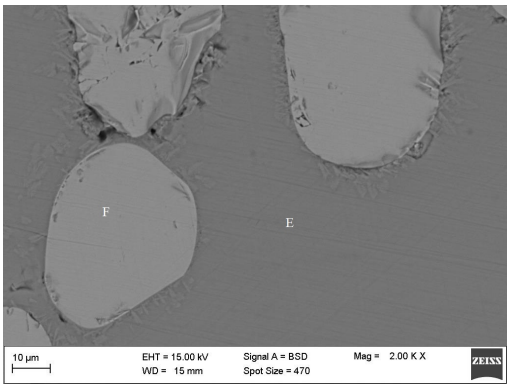

(b) 1000 °C

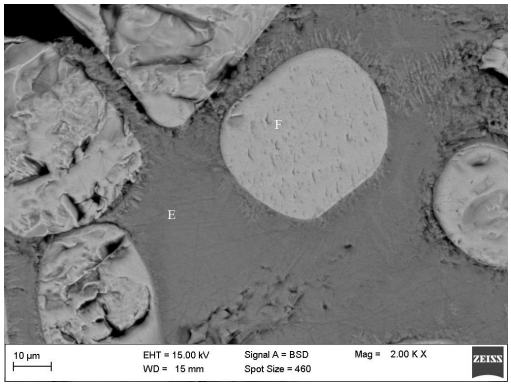

(c) 1200 °C

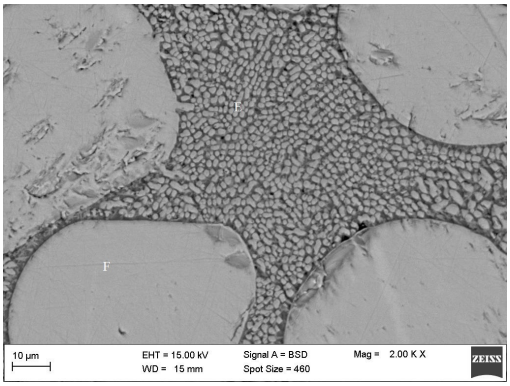

(d) 1400 °C

Figure 4: BSE micro-images of quenched samples: light crystals in (a) are $FeVO_4$(s)(E) and non-crystalline dark glassy phase is molten slag (F). For, (b),(c) and (c) light crystals are hematite solid solution (E) and lighter crystalline phases embedded in the molten slag are precipitate from quenching.

tation is observed in the molten slag phase attributed by an increase of Fe concentration. This unusual phenomenon indicates that quenching was not fast enough. This light grey precipitate particulates have a significantly higher Fe concentration than the darker glassy phase. The amount of precipitation significantly increases for a sample quenched at 1400 °C. In other words, an increase of Fe solubility in the slag enhanced precipitation. Moreover, reducing sample size to less than 0.2 g and quenching a sample in brine did not reduce precipitation. The larger grains are Fe_2O_3(s) that have a V concentration less than 5 wt.% for all samples quenched.

Albeit some uncertainty exist at temperatures at and above 1400 °C, no liquidus data above 1400 °C could be found in literature and subsequently experimental data had to be accepted and used for the assessment. Until now and to our best knowledge, no better experimental technique has been developed to quantitatively investigate element distribution among phase assemblage of oxide systems within this temperature range. Other unusual analytical approaches followed for our system include:

- Due to precipitation within the slag phase (light grey particulates embedded in dark glassy phase), the spotsize of the electron probe was increased from 5 to 10 μm for samples above 1200 °C. The idea was to analyse a larger area (field analysis) within the slag phase to estimate some average composition between the glassy phase and precipitate. Up to 15 spots within the slag phase were analysed. This technique, although not standard practice, was successful, as calculated standard deviations for Fe and V were only slightly higher than 1%, except for the sample quenched at 1400 °C (See Table 4). The latter had standard deviations larger than 5% for both Fe and V, respectively.

- More liquid phase had to be produced to have enough liquid areas larger than 10 μm in diameter within the sample, to allow for a probe spotsize of 10 μm. However, the slag behaved aggressively at temperatures above 1400 °C and it became increasingly difficult to contain the sample. Furthermore, excessive precipitation from the slag phase made it impossible to estimate Fe and V composition within acceptable error limits. Consequently, liquidus composition couldn't be estimated at and above 1450 °C.

Although not compelling, the ratio of Fe to O at 1450 °C constitutes that of hematite and not spinel, suggesting that hematite is stabilised by the dissolved V, when compared to pure hematite transition temperature to spinel (See Equation 2). However, it is possible that an equilibration time of 4 hours may not have been long enough to allow for this transition to occur. A further investigation into this phenomena might be required to confirm the findings from this study.

6.2. Thermodynamic Calculations

Based on all normalized experimental data, the thermodynamic properties and optimized model parameters for all phases in the Fe-V-O system in air are presented in Table 5 and Table 6. With these parameters, phase equilibria, invariant reactions and thermodynamic properties were calculated and compared with available literature data.

Phase diagrams, calculated from optimized parameters are shown in Figure 5. All the experimental data superimposed onto the diagram were considered during optimization. It is observed that the experimental liquidus and solidus data are well reproduced by the calculation. However, the liquidus compositions deviate marginally from the results of this study, since experimental data from Walczak et al. [2], Fotiev et al. [1] were also considered with equal weight contribution.

For the quasichemical model, two parameters were required to reproduce the liquidus. Since, $FeVO_4$ and $Fe_2V_4O_{13}$ do not melt congruently, the influence of the $\Delta g^{\circ}_{Fe-V_2O_3}$ is small compared to $g^{10}_{Fe^{3+}-V_2O_3}$ and $g^{01}_{Fe^{3+}-V_2O_3}$. No parameters were required for the quasichemical reaction between $V_2O_3^{4+}$ and Fe^{2+}, because Fe^{2+} concentration is very low at oxidizing conditions.

Two parameters were also required when the liquidus was described with the associate species model. However, one less coefficient was in fact required to reproduce experimental data within similar error limits compared to when the MQM was used to describe the slag phase.

The calculated invariant reactions (Table 7) are in good agreement with the experimental results from this study and the studies of Fotiev et al. [1], Walczak et al. [2]. For the Hematite solid solution, the enthalpy of formation and standard entropy of compound V_2O_5(s) were optimized and then added to $G^0_{V_2O_5(s)-Hem}$ to have a good agreement with the solidus compositional experimental results from this study.

Table 5: Calculated enthalpies and entropies of pure compounds in the Fe-V-O system compared with the experimental data.

Compound	$\Delta H^{\circ}_{f,298}$ J.mol^{-1}	S°_{298} Jmol^{-1}K^{-1}	a	b	c	d	e	C_p range K	Reference
Solids									
Fe_2O_3(s)*	-825787.0	87.7285	137.01				-29.07640	298-2500	[60]
V_2O_5(s)	-1550590	130.559	25.970	50.00	5853.80	-76.76761	-7.541627	298- 943	[60]
$FeVO_4$(s)	-1186800	128.400	129.51	24.71			-21.60000	298 - 973	[29]
”	-1184723	128.436	”	”			”	298 - 1173	Using MQM
”	-1185083	127.981	”	”			”	298 - 1173	Using ASM
$Fe_2V_4O_{13}$(s)	-3934650	385.700	388.83	73.83			-65.06000	298 - 973	[29]
”	-3937787	382.628	”	”			”	298 - 973	Using MQM
”	-3940147	379.761	”	”			”	298 - 973	Using ASM
Liquid									
V_2O_5(l)	-1491202	191.958	164.31	24.00			-36.28207	298 - 600	[60]
			190.79					600 - 3000	[60]
FeO(l)	-234643.2	78.4655	-18.024	31.00	1500.90		-25.33300	298 - 1644	[60]
			68.199					1644 - 2000	[60]
Fe_2O_3(l)	-728657.5	146.050	137.01				-29.07640	298 - 2500	[33]
”	-745158.3	139.467	”				”	298 - 2500	Using MQM
”	-711417.9	159.910	”				”	298 - 2500	Using ASM

$$Cp(J.mol^{-1}K^{-1}) = a + b(10^{-3})T + cT^{-0.5} + d(10^{3})T^{-1} + e(10^{5})T^{-2}$$

*Hematite exhibits magnetic ordering and these values include the magnetic contribution.

Table 6: Optimized parameters of solutions in the Fe-V-O system in air.

Liquid: FeO-Fe_2O_3-V_2O_5

Quasichemical Model (Figure 5a)
FeO-Fe_2O_3 binary parameters
Taken from the study of Degterov et al. [21]
V_2O_5-Fe_2O_3 binary parameters

$$Z_{Fe^{2+}} = 1.37, Z_{Fe^{3+}} = 2.0661, Z_{V_2O_3^{4+}} = 2.7548$$

$$g^{10}_{Fe^{3+}-V_2O_3} = -58127.5 + 33.8728T^{1}$$

$$g^{01}_{Fe^{3+}-V_2O_3} = -13515.57$$

Associate Species Model (Figure 5b)
FeO-Fe_2O_3 binary parameters
Taken from the study of Kowalski and Spencer [33]
V_2O_5-Fe_2O_3 binary parameters

$$^{0}L_{V_2O_5-Fe_2O_3} = -31308.9$$

$$^{1}L_{V_2O_5-Fe_2O_3} = 20.2411T$$

Hematite Solid Solution

For MQM - $G^{0}_{V_2O_5(s)-Hem} = G^{0}_{V_2O_5(s)} - 219004 + 94.629T - 18.651T$ from 298 - 1723 K

For ASM - $G^{0}_{V_2O_5(s)-Hem} = G^{0}_{V_2O_5(s)} - 219250 + 93.832T - 18.651T$ from 298 - 1723 K

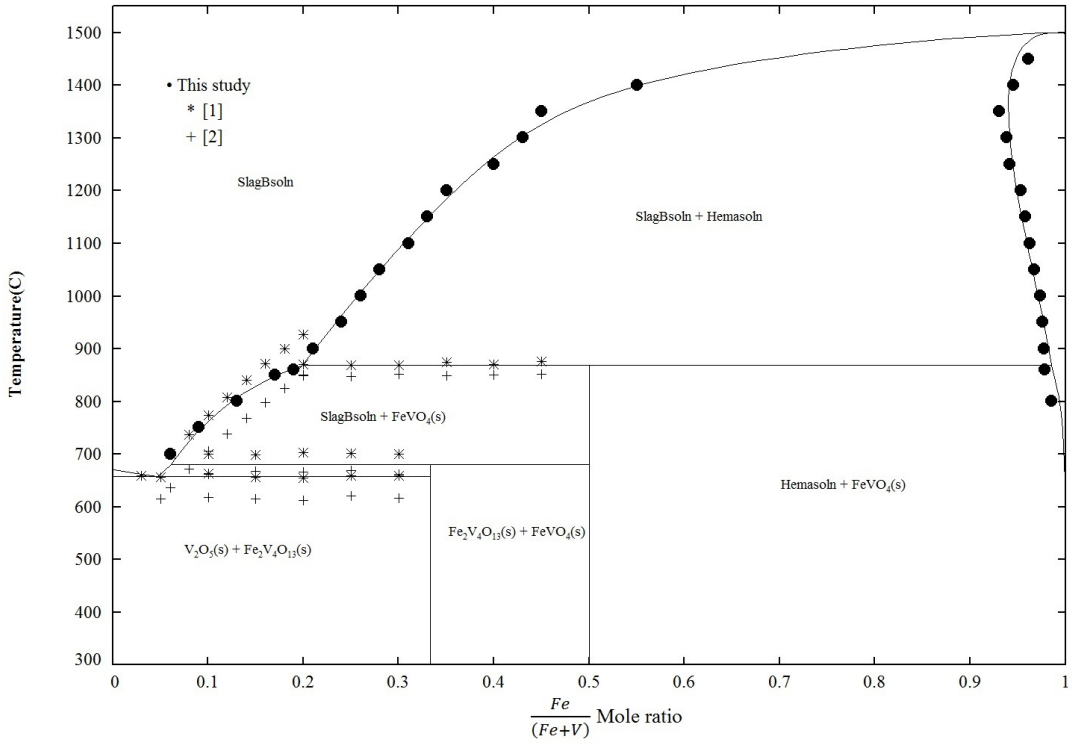

(a) Slag phase calculated with Qausichemical model

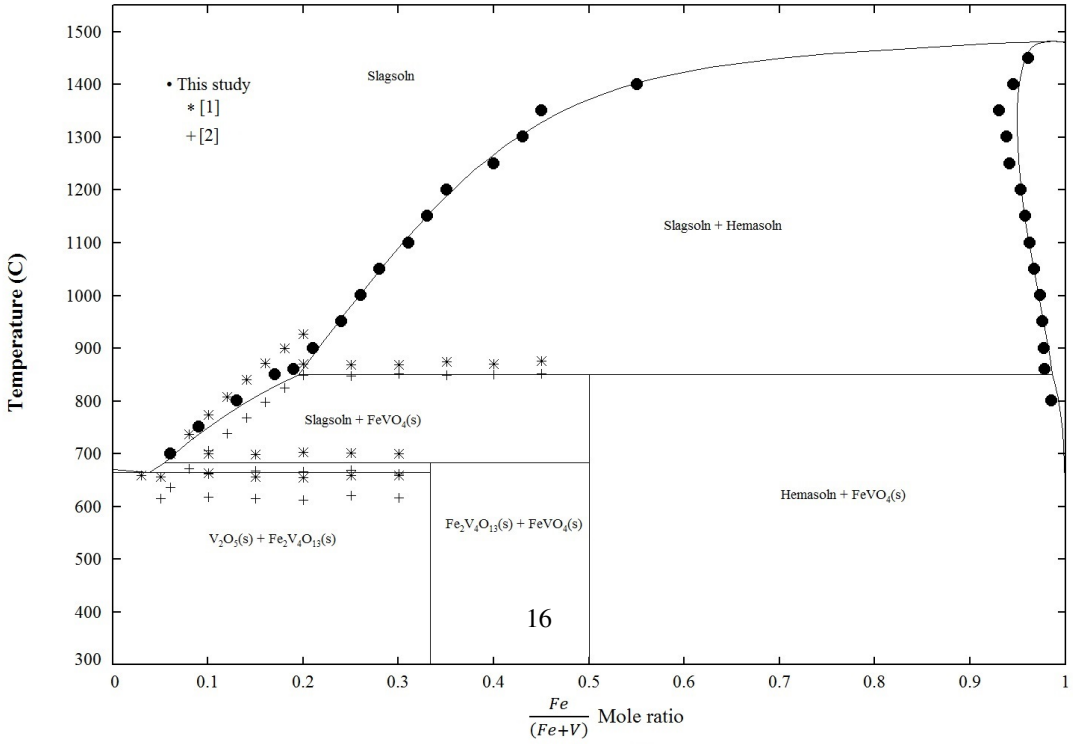

(b) Slag phase calculated with associate species model

Figure 5: Equilibrium phase diagrams of the Fe-V-O system in air

Table 7: Invariant reactions and phase transitions in the Fe−V−O system in air from calculations.

Model for liquid phase	Composition (V_2O_5 mole %)	Temperature °C	Type of invariant	Equilibrium solid phases
MQM	96	656	Eutectic	V_2O_5, $Fe_2V_4O_{13}$
ASM	97	663	Eutectic	V_2O_5, $Fe_2V_4O_{13}$
MQM	94	680	Peritectic	$FeVO_4$, $Fe_2V_4O_{13}$
ASM	95	685	Peritectic	$FeVO_4$, $Fe_2V_4O_{13}$
MQM	80	867	Peritectic	$FeVO_4$, Fe_2O_3
ASM	80	863	Peritectic	$FeVO_4$, Fe_2O_3

Both liquid models successfully described the liquidus composition, which is an indication that both models can be employed to make accurate predictions of the liquid phase. Moreover, the versatility and flexibility of both models are demonstrated and it can not be said that one model is superior to the other, given that both models only required two parameters to reproduce the liquidus data from this study.

The assessment had successfully covered all compounds and solutions up to 1450 °C. Due to the lack of experimental data at and above 1450 °C it had to assume that the solid state transition of hematite to spinel or magnetite does not take place. That said, spinel was not included in the final calculation and the melting point of pure hematite shown on both phase diagrams is not entirely correct. The calculated liquidus and solidus compositions above 1400 °C and 1450 °C are from extrapolation of the model equations and in reality, a transition is likely to occur at some temperature above 1450 °C. Moreover, some vanadium is also likely to report to spinel, which in turn can influence the transition temperature of this hematite solid solution to spinel.

7. Conclusions

The solutions and compounds in the Fe-V-O system were successfully characterized by means of equilibration/quench/analysis. The orthovanadate, $Fe_2V_4O_{13}$(s) was synthesized and identified with SEM-EDS. The slow formation of $Fe_2V_4O_{13}$(s) contributed to why some authors did not detect it. The liquidus and solidus compositions in the Fe rich section were determined experimentally and analysed with EPMA. A coexistence of a homogeneous liquid phase and orthovanadate, $FeVO_4$(s) at and below 850 °C was observed. Above 860 °C, $FeVO_4$(s) decomposed into Fe_2O_3(s) and liquid. Very little precipitation was observed within the liquid phase at 1000 °C, but precipitation increased from 1200 °C to 1400 °C. Precipitation was not subdued by a smaller sample size or a brine quenching medium. Consequently, calculated standard deviation of Fe and V increased with more precipitation. Nevertheless, standard deviation of the liquid phase was still below or just marginally above 2 % for most samples quenched below 1400 °C.

A thermodynamic assessment was conducted on the basis of phase equilibria results from this and other studies. The modified quasichemical and associate species model were used to describe the properties of the liquid. The solubility of vanadium in hematite was developed within the framework of the compound energy formalism. Two sets of consistent thermodynamic parameters were obtained. Moreover, both liquid models required two parameters to reproduce liquidus data and calculated phase diagrams showed good agreement with experimental data. However, more experimental data was required to determine the transition temperature of vanadium solubility in spinel. All calculated liquidus data above 1400 °C were extrapolated based on the assumption that no vanadium had dissolved in spinel. It is therefore our recommendation that an experimental technique, which overcomes difficulties from excess precipitation associated with this system, is developed to obtain liquidus and solidus data above 1400 °C.

8. Acknowledgements

This work was supported financially by the Glencore Chair in Pyrometallurgical Modelling at the University of Pretoria. We would also like to give gratitude to Prof Pekka Taskinen at Aalto University, School of chemical Engineering for lending their facilities to carry out experimental work. The authors of this work would further like to thank Dr Christian Reinke at the University of Johannesburg for his assistance and cooperation with EPMA work.

A. Supplementary information

The raw data required to reproduce these findings are available to download from [https://data.mendeley.com/submissions/evise/edit/2sz4bvt4tn?submission_id=S0364-5916(18)30084-1&token=7b1615ca-a331-4900-9013-7e3d48f667af]. The processed data required to reproduce these findings are available to download from [https://data.mendeley.com/submissions/evise/edit/2sz4bvt4tn?submission_id=S0364-5916(18)30084-1&token=7b1615ca-a331-4900-9013-7e3d48f667af].

References

[1] A. A. Fotiev, S. M. Cheshnitskii, L. L. Surat, The Thermal Properties of Iron Orthovanadate, Russ. J. Inorg. 28 (4) (1983) 560–562.

[2] J. Walczak, J. Ziolkowski, M. Kurzawa, J. Osten-Sacken, M. Lysio, Studies on Fe_2O_3-V_2O_5 system, Pol. J. Chem. 59 (3) (1985) 255–262.

[3] N. Lebrun, P. Perrot, Refroctory metal systems: Phase diagrams, Crystollographic and thermodynamic data, vol. 11E3, Springer Berlin Heidelberg, URL http://dx.doi.org/10.1007/978-3-642-00771-2_25, 2010.

[4] A. Burdese, The System Fe_2O_3-V_2O_5, Ann. Chim. (Rome) 47 (7-8) (1957) 797–805.

[5] R. C. Kerby, J. R. Wilson, Solid-Liquid phase equilibria for the ternary systems, V205 - Na20 - Fe203, V205 - Na20 - Cr2O3 and V205 - Na20 - MgO, Can. J. Chem. 51 (7) (1973) 1032–1040, URL http://dx.doi.org/10.1139/v73-153.

[6] E. Jak, P. Hayes, Phase Equilibria determination in complex slag systems, Mineral Processing and Extractive metalllurgy: Transactions of the institutions of Mining and Metallurgy 117 (1) (2008) 1–17, URL http://dx.doi.org/10.1179/174328508X272344.

[7] C. Bale, P.Chartrand, S. Degterov, G.Eriksson, K.Hack, R. Mahfoud, J. Melancon, A. Pelton, S.Petersen, FactSage thermochemical software and databases, CALPHAD: Computer Coupling of Phase Diagrams and Thermochemistry 26 (2) (2002) 189–228, URL http://dx.doi.org/10.1016/S0364-5916(02)00035-4.

[8] B. Slobodin, A. Fotiev, I. Miller, The Thermal Properties of Iron Orthovanadate, Russ. J. Inorg. Chem. 21 (2) (1976) 175–178.

[9] E. Burzo, L. Stanescu, V. Teodorescu, I. Ardelean, M. Coldea, Some physical properties of $V_2O_5-Fe_2O_3$ and $V_2O_5-Fe_2O_3-Li_2O$ systems, J. Mater. Sci. 13 (9) (1978) 1855 – 1867.

[10] J. Muller, J. Joubert, Synthesis of a High Pressure High Temperature Form of Dense $FeVO_4$ and Evidence for an Allotropic Form of the $CrVO_4$ type, J. Solid State Chem 14 (1975) 8 – 13, URL http://dx.doi.org/10.1016/0022-4596(75)90355-2.

[11] Y. Hotta, Y. Ueda, N.Nakayama, K. Kosuge, S. Kachi, M. Shimada, M. Koizumi, Pressure-Products Diagram of $Fe_xV_{1-x}O_2$ System ($0 < x$ 0.5), J.Solid State Chem. 55 (3) (1984) 314 – 319, URL http://dx.doi.org/10.1016/0022-4596(84)90283-4.

[12] R. Pletnev, A. Fotiev, V. Lisson, Phase composition of the $Fe_2O_3-V_2O_5$ system, Russ. J. Inorg. Chem. 20 (3) (1975) 1356 – 1357.

[13] L. Permer, Y. Laligant, Crystal structure of the Tetrapolyvanadate $Fe_2V_4O_{13}$, Eur. J. Solid State Inorg. Chem. 34 (1997) 41 – 52.

[14] X. Wang, K. Heier, C. Stern, K. Poeppelmeier, Structure comparison of iron tetrapolyvanadate $Fe_2V_4O_{13}$ and iron Polyvanadomolybate $Fe_2V_3 \cdot 16\,Mo_0 \cdot 84\,O_{13} \cdot 42$: A new substitution mechanism of molybdenum VI for vanadium V, Inorg. Chem. 37 (26) (1998) 6921–6927.

[15] Y. Si, L.Zhao, Z.Yu, W. Wang, J.Qiuh, Y.Yang, A novel amorphous $Fe_2V_4O_{13}$ as cathode material for lithium secondary batteries, Materials Letters 27 (2012) 145–147, URL http://dx.doi.org/10.1016/j.matlet.2011.12.104.

[16] C. Alcock, C. Ji, Vanadium-oxygen system. A Review, High Temperature - High Pressures 22 (2) (1990) 139 – 147.

[17] H. Wriedt, The O-V Oxygen - Vanadium system, Bulletin of Alloy Phase Diagrams 10 (3) (1989) 271 – 277, URL http://dx.doi.org/10.1007/BF02877512.

[18] Y. Kang, Critical evaluation and thermodynamic optimization of the VO - $VO_2 \cdot 5$, Journal of the European Ceramic Society 32 (2012) 3187 – 3198, URL http://dx.doi.org/10.1016/j.jeurceramsoc.2012.04.45.

[19] Y. Yang, H. Mao, M. Selleby, Thermodynamic assessment of the V-O system, CALPHAD: Computer Coupling of Phase Diagrams and Thermochemistry 51 (2015) 144–160, URL http://dx.doi.org/10.1016/j.calphad.2015.08.003.

[20] P. WU, G. Eriksson, A. Pelton, M. Blander, Prediction of the thermodynamic properties and phase diagrams of silicate systems - evaluations of the FeO-MgO-SiO_2systems, ISIJ international 33 (1) (1993) 26 – 35, URL http://dx.doi.org/10.2355/isijinternational.33.26.

[21] S. A. Degterov, E. Jak, P. Hayes, A. D. Pelton, Experimental study of phase equilibria and thermodynamic optimization of the Fe-Zn-O system, Metallurgical and Materials Transactions B 32 (B) (2001) 643–657, URL http://dx.doi.org/10.1007/s11663-001-0119-2.

[22] T. Hidayat, D. Shishin, E. Jak, S. Decterov, Thermodynamic reevaluation of the Fe-O system, CALPHAD: Computer Coupling of Phase Diagrams and Thermochemistry 48 (2015) 131 – 144, URL http://dx.doi.org/10.1016/j.calphad.2014.12.005.

[23] H. Lukas, S. Fries, B. Sundman, Computational thermodynamics, the Calphad method, Cambridge University press, Cambridge, UK, 2007.

[24] R. Shannon, Revised effective ionic radii and systematic studies of interatomic distances in halides and chalcogenides, Acta Crystallogr A. 32 (1976) 751–767, URL https://doi:10.1107/S0567739476001551.

[25] E. Burzo., L. Stanescu, Crystallographic Investigation of the V_2O_5 - Fe_2O_3 solid solution Using MÃűssbauer Effect, Solid State Commun. 20 (7l) (1976) 653–655.

[26] E. Burzo., L. Stanescu, On the Charge Compensation of Iron Ions in V_2O_5 Lattice, Phys. Status Solidi A. 46 (2l) (1978) K163–K166.

[27] O. Palanna, A. Mohanand, A. Biswas, Electrical Properties of Fe_2O_3-V_2O_5 System, Proc. Indian Acad. Sci. A 87 (8l) (1978) 259–265.

[28] Y. Otsubu, K. Utsumi, Thermochemical properties of $Fe_2O_3 \cdot 2\,V_2O_5$ in the iron oxide-vanadium pentoxide system, Nippon Kagaku Zasshi 92 (8) (1971) 737.

[29] V. Volkov, Equilibrium diagram and thermodynamic charateristics of vanadates of the $V_2O_5-Fe_2O_3-VO_2$ system, Russ. J. Inorg. Chem. 24 (4) (1979) 1062–1066.

[30] Y. Kesler, S. Cheshnitskii, A. Fotiev, Y. Tretyakov, Enthalpy of formation of vanadates of iron, chromium and aluminium, Inorg. Mater. 21 (4) (1985) 649–651.

[31] S. Cheshnitski, V. Kozhevnikov, A. Fotiev, Heat capacity of ferrous orthovanadate in the range from 5 to 300 K, Inorg. Mater. 21 (4) (1985) 594–595.
[32] A. Borukhovich, I. Miller, M. Marunya, A. Fotiev, Heat Capacity of Iron, Chromium, and Nickel Orthovanadates, Russian Journal of Inorganic chemistry 11 (5) (1975) 830–831.
[33] M. Kowalski, P. Spencer, Thermodynamic reevaluation of the Cr-O, Fe-O and Ni-O systems: Remodelling of the liquid, BCC and FCC phases, CALPHAD: Computer Coupling of Phase Diagrams and Thermochemistry 19 (3) (1995) 229 – 243, URL http://dx.doi.org/10.1016/0364-5916(95)00024-9.
[34] R. Robert, CRC Handbook of Chemistry and Physics, vol. 62, Boca Raton, FL: CRC Press, Cambridge, UK, URL ISBN0-8493-0462-8, 1981.
[35] C. Merlet, An Accurate Computer Correction Program for Quantitative Electron Probe Microanalysis, Mikrochim.Acta 114/115 (1994) 363–376.
[36] T. I. Barry, A. T. Dinsdale, J. Gisby, Predictive thermochemistry and phase equilibria of slags, Review of extraction & processing 45 (4) (1993) 32–38, URL https://doi.org/10.1007/BF03223284.
[37] M. Koretsky, Engineering and chemical thermodynamics, vol. 1, John Wiley and Sons, Inc., 111 River Street, Hoboken, NJ 07030, 2004.
[38] A. Pelton, M. Blander, Thermodynamic Analysis of Ordered Liquid Solutions by a Modified Quasi-Chemical Approach - Application to Silicate Slags, Met. Trans. B 17B.
[39] A. Pelton, M. Blander, Thermodynamic Analysis of Binary-Liquid Silicates and Prediction of Ternary Solution Properties by Modified Quasi-Chemical Equations, Geochim. Cosmochim. Acta 51 (1987) 85–95.
[40] W. Xie, N.Wang, Z. Qiao, Z. Cao, Thermodynamic assessment of the PbO - V_2O_5 system, CALPHAD: Computer Coupling of Phase Diagrams and Thermochemistry URL http://dx.doi.org/10.1016/j.calphad.2016.04.005.
[41] Y. Kawakita, H. Nakashima, S. Yoshioka, S. Takeda, K.Maruyama, M. Inui, K. Tamura, Local structures of liquid and vitreous V_2O_5 and P_2O_5, Journal of Physics and Chemistry of Solids 60 (1999) 1483 – 1486, URL http://dx.doi.org/S0022-3697(99)00148-1.
[42] S. Hawakawa, T. Yoko, IR and NMR structural studies on lead vanadate glasses, Journal of non-crystalline solids 183 (1995) 73–84.
[43] P. Hudon, I. Jung, Critical evaluation and thermodynamic optimization of the $CaO-P_2O_5$ system, Metallurgical and Materials Transactions B 46 (B) (2014) 494–522.
[44] M. Rahman, P.Hudon, I. Jung, A coupled experimental study and thermodynamic modelling of the $SiO_2-P_2O_5$ system, Metallurgical and Materials Transactions B 44 (B) (2013) 837–852.
[45] G. Eriksson, A. Pelton, G. Eriksson, S. A. Degterov, C. Robelin, Y. Dessurrault, The Modified Quasichemical Model I-Binary Solutions, Metallurgical and Materials Transactions B 31 (B) (2000) 651–659, URL http://dx.doi.org/10.1007/s11663-000-0103-2.
[46] N.Wang, Critical evaluation and thermodynamic assessment of the $CaO-MgO-V_2O_5$ system, M.sc. thesis, University of Science and Technology, Beijing, 2015.
[47] V. Protstakova, J.Chen, E.Jak, S. Decterov, Experimental investigation and thermodynamic modelling of the $(NiO+CaO+SiO_2)$ and $(NiO+CaO+MgO+SiO_2)$, J. Chem. Thermodynamics 86 (B) (2015) 130–142, URL http://dx.doi.org/10.1016/j.jct.2015.01.017.
[48] A. Pelton, A general "Geometric" thermodynamic model for multicomponent solutions, CALPHAD: Computer Coupling of Phase Diagrams and Thermochemistry 25 (2) (2001) 319–328, URL https://doi.org/10.1016/S0364-5916(01)00052-9.
[49] I. Jung, S. Deceterov, A. Pelton, Critical thermodynamic optimization of the Fe-Mg-O system, Journal of Physics and Chemistry of Solids 65 (1) (2004) 1683–1695, URL http://dx.doi.org/10.1016/j.jpcs.2004.04.005.
[50] W. Zhang, M. Chen, Thermodynamic modelling of the Co-Fe-O system, CALPHAD: Computer Coupling of Phase Diagrams and Thermochemistry 41 (1) (2013) 76–88, URL http://dx.doi.org/10.1016/j.calphad.2013.02.002.
[51] V. Prostakova, J.Cheng, E.Jak, S. Decterov, Experimental investigation and thermodynamic modeling of the $NiO-CaO-SiO_2$, NiO-CaO-SiO2 and $NiO-CaO-MgO-SiO_2$ systems, Journal of chemical thermodyanamics 86 (2015) 130–142, URL http://dx.doi.org/10.1016/j.jct.2015.01.017.
[52] J. W. Hastie, D. W. Bonnell, A Predictive Phase-Equilibrium Model for Multicomponent Oxide Mixtures. 2. Oxides of Na-K-Ca-Mg-Al-Si, High Temp. Sci. 19 (3).
[53] J. W. Hastie, New Techniques and Opportunities in High-Temperature Mass Spectrometry, Pure Appl. Chem. 56 (11).
[54] J. W. Hastie, E. R. Plante, D. W. Bonnell, Vaporization of Simulated Nuclear Waste Glass, NBSIR 83-2731 NIST.
[55] D. W. Bonnell, J. W. Hastiel, A Predictive Thermodynamic Model for Complex High-Temperature Solution Phases, High Temp. Sci. 26 (313).
[56] M. Hillert, L. Staffansson, The Regular Solution Model for Stoichiometric Phases and Ionic Melts., Acta Chem. Scand. 24 (1970) 3618–3626, URL http://dx.doi.org/10.3891/acta.chem.scand.24-3618.
[57] B. Sundman, J. Agren, A regular solution model for phases with several components and sublattices, suitable for computer applications., Journal of Physics and Chemistry of Solids 42 (4) (1981) 297âĂŞ301, URL http://dx.doi.org/10.1016/0022-3697(81)90144-X.
[58] T. Zieniert, O. Fabrischnaya, Thermodynamic assessment and experiments in the system $MgO-Al_2O_3$, CALPHAD: Computer Coupling of Phase Diagrams and Thermochemistry 40 (2015) 1–9, URL http://dx.doi.org/10.1016/j.calphad.2012.10.001.
[59] D. Newbury, N. Ritchie, Performing elemental microanalysis with high accuracy and high precision by scanning electron microscopy/silicon dirft detector energy-dispersive X-ray spectrometry, Journal of Material Science 50 (2015) 493–518, URL http://dx.doi.org/10.1007/s10853-014-8685-2.
[60] C. Bale, E.Belisle, P. Chartand, S. Decterov, G. Eriksson, K. Hack, I. Jung, Y. Kang, J. Melancon, A. Pelton, C. Robelin, S. Petersen, FactSage thermochemical sofware and databases - recent developments, CALPHAD: Computer Coupling of Phase Diagrams and Thermochemistry 33 (2) (2009) 295âĂŞ311, URL https://doi.org/10.1016/j.calphad.2008.09.009.